

# Information spreading and scrambling in disorder-free multiple-spin interacting models

Yoshihito Kuno<sup>1</sup>, Takahiro Orito<sup>2</sup>, and Ikuo Ichinose<sup>3</sup>

<sup>1</sup>*Graduate School of Engineering Science, Akita University, Akita 010-8502, Japan*

<sup>2</sup>*Graduate School of Advanced Science and Engineering, Hiroshima University, 739-8530, Japan and*

<sup>3</sup>*Department of Applied Physics, Nagoya Institute of Technology, Nagoya, 466-8555, Japan*

(Dated: March 31, 2022)

Tripartite mutual information (TMI) is an efficient observable to quantify the ability of scrambler for unitary time-evolution operator with quenched many-body Hamiltonian. In this paper, we give numerical demonstrations of the TMI in disorder-free (translational invariant) spin models with 3-body and 4-body multiple-spin interactions. The dynamical behavior of the TMI of these models does *not* exhibit linear light-cone. In early-time evolution, the TMI displays distinct negative increase behavior fitted by a logarithmic-like function. This is in contrast to the conventional linear light-cone behavior present in the XXZ model. The late-time evolution of the TMI in finite-size systems is also numerically investigated. The results indicate that the saturation values of the TMI have correlations with nearly integrable properties of the system estimated by the level spacing analysis. These multiple-spin interactions make the system nearly integrable and weakly suppress the spread of information and scrambling.

## I. INTRODUCTION

Characterization of quantum chaos and scrambling (spread of information) [1, 2] is a topic of great interests in broad physical fields from high-energy, condensed matter to information physics. How information in a subsystem of an initial state spreads across the entire system through a quantum channel is currently studied extensively. In high energy physics, it was clarified that black hole has the most efficient ability of scrambling, spread of quantum information [2–4]. In condensed matter physics, on the other hand, how a many-body Hamiltonian, describing condensed matter phenomena, stirs quantum states under time evolution is a frequently asked question [5, 6]. In other words, which properties of the many-body Hamiltonian control the degree of spread of information is currently one of the most important topics of quantum physics. As typical examples, it is believed nowadays that Anderson localized system strictly inhibits the spread of information and scrambling, and certain many-body localized systems also exhibit a similar nature [5–7]. The above observation has been elucidated by studying the time evolution of bipartite entanglement entropy (BEE) [8]. The notion of spread of information and scrambling is expected to be related to thermalization of the system [9, 10], which is also an attractive topic in both high-energy and condensed matter physics. Intuitively, the realization of thermalization corresponds to the full spread of information and scrambling over the entire system under consideration, although there is no exact proof of it.

So far, as an efficient tool to measure the spread of information and scrambling in many-body systems, the out-of-time-ordered-correlation (OTOC) was proposed in [3, 4]. The OTOC is an operator-based quantity to quantify the spread of information and scrambling. The OTOC has been applied to various condensed matter systems, e.g., disordered system [11–14] and some specific

systems [15–21].

Besides the OTOC, another quantity was proposed to quantify the degree of scrambling, which extracts the scrambling ability of the operator of the quantum channel itself: The tripartite mutual information (TMI) of a dual pure state obtained by the state-channel map, proposed by Hosur, et.al. [22]. The negativity of the TMI indicates the non-locality of information, i.e., the spread of information and scrambling across the entire system. The TMI is an efficient quantitative diagnostic of the spread of information and scrambling especially for unitary time-evolution operator  $U(t) = e^{-itH}$ , where  $H$  is a many-body Hamiltonian. We note that a choice of observable is needed for calculating the OTOC, but for the TMI, it is not. Also, the time evolution of the TMI is essentially different from that of the BEE for a certain initial state set, which is often measured in the dynamics of many-body quantum states.

While we often take ensemble of random initial product states in the conventional measure of the BEE, the calculation of the TMI does not require that procedure. The spread of information and scrambling may be well observed not as the dynamics of the many-body wavefunction, but as one of the properties of time-evolution operator of a many-body Hamiltonian [23]. However, the study of the systematic observation of the TMI for various many-body systems is still lacking. It is therefore important to investigate how scrambling changes with the different physical properties of individual models by observing the TMI and to clarify relevant ingredients for scrambling.

In this paper, we shall study the TMI for disorder-free spin models with multiple-spin interactions. That is, two types of model are investigated, which are generalizations of the standard  $s = \frac{1}{2}$  XXZ spin model: (I) Spin model with 3-body interactions; (II) Model including 4-range multiple-spin interactions. In the previous study [24], the BEE was studied for similar models to the above by

employing a specific type of initial state, and the emergence of slow thermalization was observed there. However, knowledge of how the quench time-evolution operator influences (enhances or suppresses) the spread of information and scrambling is still lacking, and we shall study that problem by means of observing the TMI. Also, a recent study [25] gave a general classification for the late time dynamics of the TMI in various types of model. From a general point of view, however, how the nature of integrability and dynamics of the TMI are related to each other is an open problem. In fact, recent numerical calculations of the late time value (saturation value) of the TMI in certain models [26–28] indicate no correlations between them, while other studies of the TMI for the many-body localized (MBL) systems [29, 30] imply the existence of certain relationship between the integrability of the system and the behavior of the TMI. Therefore, a detailed study of the dynamics of the TMI in various concrete quantum many-body models is desired to understand quantum information scrambling.

Motivated by the above observations, we shall investigate the behavior of the TMI for the specific 3-body and 4-range models. In particular, as the target models reduce to the integrable XXZ model for the vanishing multiple-spin interactions and also they acquire integrability for the strong-coupling limit, the present study on the models reveals some properties of the phases in the vicinity of integrability, and it may also give useful insight into finite-size (intermediate) MBL regime and chaos due to breaking integrability, which were proposed recently [31, 32]. Besides these works, there appeared several interesting studies on weakly broken integrability phenomena these days [33–37], whose relationship with the present work is an interesting future problem.

In this paper, by the numerical study of the TMI, we obtain the following two observations: (I) For the standard XXZ model, the TMI in early-time evolution exhibits linear light-cone spread. On the other hand for the models with multiple-spin interactions, we find that the decrease of the TMI (an increase of the absolute value of the TMI) in early-time evolution is fitted in a logarithmic-like function of time, that is, the multiple-spin interactions change the behavior of the TMI. (II) We investigate the late-time evolution of the TMI. The present finite-size system calculation indicates that the near integrability of the model, which is revealed by the level spacing analysis (LSA), correlates well to the scrambling nature characterized by the late time saturation value of the TMI.

The rest of this paper is organized as follows. In Sec. II, we introduce the TMI and explain the methods for the practical calculation. In Sec. III, we introduce the target disorder-free spin models and also briefly explain their physical properties, which have been revealed by the previous work. In Sec. IV, we show the numerical calculations of the TMI for the target spin models. In particular, the numerical results for two different time intervals are shown, i.e., early-time evolution and late-time ones.

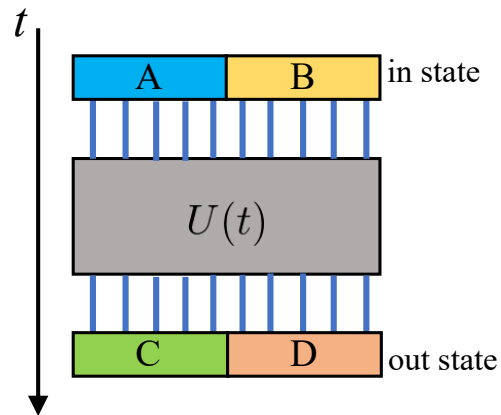


FIG. 1. Schematic image of the time evolution of the state with doubled Hilbert space. The spatial partitioning of the system is represented where four subsystems A, B, C, and D are introduced. Each part is  $L/2$ -lattice sites.

We discuss the physical meanings of the results. Section V is devoted to discussion and conclusion.

## II. CALCULATION OF TMI

In this section, we introduce the TMI proposed in [22], and briefly explain the methods of the practical numerical calculation to be applied for one-dimensional lattice models with  $L$  sites. Our numerical resource allows us to calculate the TMI up to the system size  $L = 14$  by the methods.

We investigate properties of the spread of information and scrambling embedded in the time evolution operator  $\hat{U}(t) \equiv e^{-itH}$ . In the treatment of the time-evolution operator in calculating the TMI, the state-channel map plays an essential role. Under this map, the time evolution operator  $\hat{U}(t) \equiv e^{-itH}$  is regarded as a pure state in the doubled Hilbert space,  $\mathcal{H}_D \equiv \mathcal{H}_{\text{in}} \otimes \mathcal{H}_{\text{out}}$  [22]. That is, we start from the density matrix at time  $t$ ,  $\rho(t) = \sum_{\nu=1}^{N_D} p_{\nu} \hat{U}(t) |\nu\rangle \langle \nu| (\hat{U}(t))^{\dagger}$ , where  $\{|\nu\rangle\}$  is a set of a orthogonal bases state (time independent),  $N_D$  is the dimension of the Hilbert space in the system, and an arbitrary input ensemble is tuned by parameters  $\{p_{\nu}\}$ . Then, by the state-channel map applied to this density matrix  $\rho(t)$ , the operator can be mapped into a pure state in the doubled Hilbert space,

$$\rho(t) \rightarrow |U(t)\rangle = \sum_{\mu} \sqrt{p_{\mu}} (\hat{I} \otimes \hat{U}(t)) |\nu\rangle_{\text{in}} \otimes |\nu\rangle_{\text{out}}, \quad (1)$$

where  $\hat{I}$  is the identity operator and  $\{|\nu\rangle_{\text{in}}\}$  and  $\{|\nu\rangle_{\text{out}}\}$  are the same set of orthogonal bases state, and therefore, the state is defined on the doubled Hilbert space,  $\mathcal{H}_D$ , spanned by  $\{|\nu\rangle_{\text{in}}\} \otimes \{|\nu\rangle_{\text{out}}\}$ . The time evolution operator  $\hat{U}(t)$  acts only on the out orthogonal states  $|\nu\rangle_{\text{out}}$ . Even though arbitrary input ensemble can be employed

by tuning  $\{p_\nu\}$  [22], in this work, we focus on the infinite temperature case, such as  $p_\nu = 1/N_D$ . Then, for initial state  $t = 0$ ,  $\hat{U}(0) = \hat{I}$ , the in-state and out-state are maximally entangled.

To estimate the TMI for the spread of information and scrambling in the time evolution, we introduce spatial partitioning to the pure state  $|U(t)\rangle$ . The spatial partitioning is done for both the  $t = 0$  in-state and the out-state at  $t$ . As shown in Fig. 1, the  $t = 0$  state (given by  $\rho(t = 0)$ ) is divided into two subsystems  $A$  and  $B$ , and similarly the state at time  $t$  (given by  $\rho(t)$ ) is divided into two subsystems  $C$  and  $D$ . We employ the partition with the equal length of  $A$  and  $B$  ( $C$  and  $D$ ) subsystems for the practical calculation.

Under this spatial partitioning, the density matrix of the pure state  $|U(t)\rangle \in \mathcal{H}_D$  is defined as  $\rho_{ABCD}(t) = |U(t)\rangle\langle U(t)|$ . From this full density matrix  $\rho_{ABCD}(t)$ , a reduced density matrix for a subsystem  $X$  is obtained by tracing out the degrees of freedom in the complementary subsystem of  $X$  denoted by  $\bar{X}$ , i.e.,  $\rho_X(t) = \text{tr}_{\bar{X}} \rho_{ABCD}$ . From the reduced density matrix  $\rho_X(t)$ , the operator entanglement entropy (OEE) for the subsystem  $X$  is obtained by conventional von-Neumann entanglement entropy,  $S_X = -\text{tr}[\rho_X \log_2 \rho_X]$ .

From the OEE, we define the mutual information between  $X$  and  $Y$  subsystems (where  $X, Y$  are some elements of the set of the subsystems  $\{A, B, C, D\}$ , and  $X \neq Y$ );

$$I(X : Y) = S_X + S_Y - S_{XY}. \quad (2)$$

This quantity indicates how the subsystems  $X$  and  $Y$  correlate with each other.

By using the mutual information, the TMI for the subsystems  $A, C$  and  $D$  is defined as;

$$I_3(A : C : D) = I(A : C) + I(A : D) - I(A : CD). \quad (3)$$

This quantity is a measure for how the initial information embedded in the subsystem  $A$  spreads into both subsystems  $C$  and  $D$  in the output state. If the spread of the information in  $A$  sufficiently occurs across the entire system at time  $t$ ,  $I_3(t)$  gets negative, while the mutual information keeps a non-negative value even in such a situation. Then, as proposed in Ref. [22], the TMI,  $I_3$ , can be used to quantify the degree of scrambling, i.e., the spread of information is characterized by a negative value of  $I_3$ . In general  $I_3$  is zero at  $t = 0$ , as  $|U(0)\rangle$  is the product state of the EPR pair at each lattice site. Then, if the time-evolution operator acts as a strong scrambler,  $I_3$  acquires a large negative value under the time evolution. On the other hand, if the time evolution operator does not act as a scrambler,  $I_3$  remains small. Hence,  $I_3$  is a good indicator to quantify the degree of scrambling, i.e., the spread of information. In this paper, we mostly employ the TMI to characterize the scrambling for our target models.

Here, we explain the practical numerical calculation of the TMI. The numerical cost for the straightforward manipulation of the density matrix  $\hat{\rho}_{ABCD}$  is quite high.

Instead, we make use of the singular value decomposition (SVD) to the pure state  $|U(t)\rangle$ . For a certain partitioning  $X$  and  $\bar{X}$ , the pure state is written as

$$\begin{aligned} |U(t)\rangle &= \frac{1}{N_D} \sum_{\nu} (\hat{I} \otimes \hat{U}(t)) |\nu\rangle_{\text{in}} |\nu\rangle_{\text{out}} \\ &= \frac{1}{N_D} \sum_{k_X, \ell_{\bar{X}}} U_{k_X, \ell_{\bar{X}}} |k_X\rangle_X |\ell_{\bar{X}}\rangle_{\bar{X}} \\ &\stackrel{\text{SVD}}{=} \sum_r \lambda_r^{X, \bar{X}} |r\rangle_X |r\rangle_{\bar{X}}. \end{aligned} \quad (4)$$

Here, in the second line, the input and output basis states are reassembled into basis vectors  $\{|k_X\rangle_X\}$  and  $\{|\ell_{\bar{X}}\rangle_{\bar{X}}\}$  corresponding to the spatial partition  $X$  and  $\bar{X}$ , and then, a concrete matrix representation of the operator  $(\hat{I} \otimes \hat{U}(t))$  is obtained. In the third line, we simply carry out the SVD to obtain singular values,  $\lambda_r^{X, \bar{X}}$ , and the OEE for the subsystem  $X$  is straightforwardly obtained by  $S_X = -\sum_r (\lambda_r^{X, \bar{X}})^2 \log_2 (\lambda_r^{X, \bar{X}})^2$ . Hence, from the numerical calculation of OEE, we evaluate the TMI,  $I_3$ .

In the following numerical calculations, we focus on spatially equal-partitioning case: i.e., as we briefly mentioned in the above, the subsystems  $A$  and  $B$  are defined as the  $L/2$ -site left and right subsystems in the input state, respectively, and the subsystems  $C$  and  $D$  are defined similarly as the  $L/2$ -site systems in the output state as shown in Fig. 1. We also focus on the zero magnetization sector of the Hilbert space in the choice of the set of bases  $\{|\nu\rangle_{\text{in(out)}}\}$ . Under this setup,  $S_Y$  with  $Y = A, B, C$  and  $D$  is a constant at any time, as their values are shown in Appendix A. We further set a reference frame of the TMI,  $I_3$ , as in Refs. [27, 29]. The reference frame is the value of the TMI of the Haar random unitary,  $I_3^H$ , which depends on the Hilbert space dimension of the system size  $L$  [38]. The value of  $I_3^H$  can be numerically calculated. Then, we define a normalized TMI,  $\tilde{I}_3(A : C : D)$  as follows,

$$\tilde{I}_3(A : C : D) \equiv \frac{I_3(t) - I_3(0)}{I_3^H - I_3(0)}. \quad (5)$$

In the following sections, we numerically obtain the value of  $\tilde{I}_3$ .

We here comment on the saturation of the TMI in a strong scrambling case. As explained in Ref. [22], even for strong scrambling, the TMI of the time-evolution operator without fixing magnetization sector does not reach the Haar-scrambled limit,  $\tilde{I}_3 = 1$ . Furthermore, since we focus on the zero-magnetization sector, the value of the TMI tends to be lowered by the constraint of the sector, however, nonetheless, the saturation value of the TMI exhibits the characteristic behavior depending on the model parameters as we show in the following.

### III. TARGET MODELS

In this paper, we consider three spin models: XXZ model, 3-body spin model, and 4-range model. These

$\hat{h}_\alpha$	Included terms
2-body, $\hat{h}_2$	$S_j^z S_{j+1}^z, S_j^z S_{j+2}^z, S_j^z S_{j+3}^z$
3-body, $\hat{h}_3$	$S_j^z S_{j+1}^z S_{j+2}^z, S_j^z S_{j+2}^z S_{j+3}^z, S_j^z S_{j+1}^z S_{j+3}^z$
4-body, $\hat{h}_4$	$S_j^z S_{j+1}^z S_{j+2}^z S_{j+3}^z$

TABLE I. Included terms for each  $\alpha$ -body Hamiltonian,  $\hat{h}_\alpha$ .

models are given as follows;

$$H_{\text{XXZ}} = \sum_j J_1 S_j^z S_{j+1}^z + H_{\text{hop}}, \quad (6)$$

$$H_{3\text{B}} = \sum_j J_1 S_j^z S_{j+1}^z + J_2 S_j^z S_{j+2}^z + J_3 S_j^z S_{j+1}^z S_{j+2}^z + H_{\text{hop}}, \quad (7)$$

$$H_{4\text{R}} = \sum_{\alpha=2}^4 t_\alpha \hat{h}_\alpha + H_{\text{hop}}, \quad (8)$$

where

$$H_{\text{hop}} = \frac{v}{2} \sum_j (S_j^+ S_{j+1}^- + S_j^- S_{j+1}^+),$$

and  $J_i$  ( $i = 1, 2, 3$ ) and also  $v$  in  $H_{\text{hop}}$  are parameters. The parameter  $\alpha$  in the model  $H_{4\text{R}}$  [in Eq. (8)] denotes the range of the interactions and each  $\hat{h}_\alpha$  is given in TABLE I. The XXZ model,  $H_{\text{XXZ}}$ , is a nonlocalized integrable model, and only a tiny integrability-breaking perturbation makes the model satisfy the ETH [33].

Experimentally, the 3-body model can be feasible in an effective theory of the Bose-Hubbard model describing cold atoms on a zig-zag optical lattice [39], where the 3-body terms perturbatively appear, and also the 3-body terms can be implemented experimentally in cold polar molecules [40].

For any value of  $v$ , the XXZ model  $H_{\text{XXZ}}$  is integrable. For  $v = 0$ , the remaining two models,  $H_{3\text{B}}$  and  $H_{4\text{R}}$ , are integrable since each eigenstate is characterized by on-site (local) conserved quantities, i.e., the eigenvalues  $\pm 1$  of  $\{S_j^z\}$  coming from the fact  $[H_{3\text{B}(4\text{R})}, S_j^z] = 0$  for any  $j$ . In addition, there exist multiple-site local conserved quantities such as  $S_j^z S_{j+1}^z S_{j+2}^z$  and  $S_j^z S_{j+1}^z S_{j+2}^z S_{j+3}^z$ , etc. These can be regarded as short domain wall operators. Such term may induce a quasi-localization phenomenon, namely, Hilbert space fragmentation or shattering [41–43]. The existence of the ‘hopping’  $H_{\text{hop}}$  breaks the integrability of the two models  $H_{3\text{B}}$  and  $H_{4\text{R}}$ , that is, these models with a tiny but finite  $v$  turn to non-integrable in a strict sense. Sometimes they are called nearly integrable model.

Previous study [24] showed that the 3-body and 4-range models display slow-thermalization for sufficiently small  $v$ . In particular, it was numerically demonstrated that the 3-body model exhibits a slow increase of the BEE for initial product states. The presence of the  $J_2$  and  $J_3$ -terms *hinders* the increase of the entanglement entropy. Also, interestingly enough, the early-time evolu-

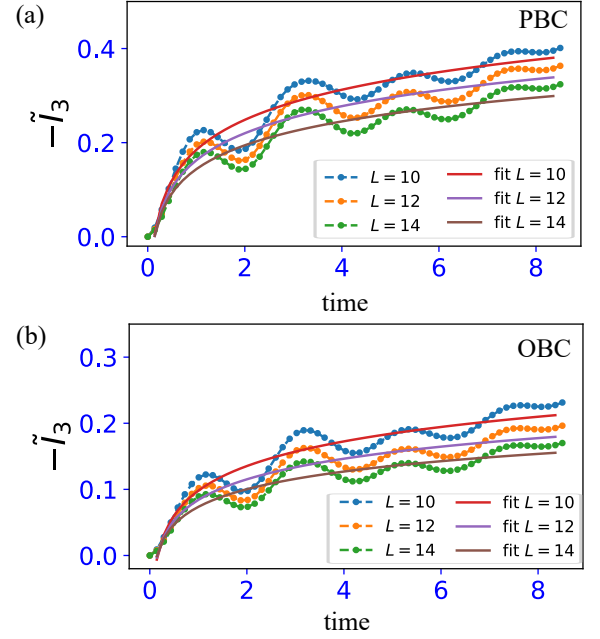


FIG. 2. Early-time evolution of 3-body model  $H_{3\text{B}}$ . (a) The result of PBC case. The logarithmic fitting lines are  $(-I_3) = 0.0639 \log_2 t + 0.184$ ,  $(-I_3) = 0.0575 \log_2 t + 0.1624$  and  $(-I_3) = 0.0507 \log_2 t + 0.1435$  for  $L = 10, 12$  and  $14$ , respectively. (b) The result of OBC case.  $(-I_3) = 0.0373 \log_2 t + 0.0970$ ,  $(-I_3) = 0.0311 \log_2 t + 0.0840$  and  $(-I_3) = 0.0267 \log_2 t + 0.0735$  for  $L = 10, 12$  and  $14$ , respectively. For both cases, we set  $J_1 = 0.3$ ,  $J_0 = 2$  and  $v = 0.2$ . In the fitting, we used the data points within  $t \in [0.1 : 8]$ .

tion of the entanglement entropy displays a logarithmic-like curve, which is in contrast to the standard linear-light cone increase in the standard XXZ model.

It is important to investigate how such a slowing-down or unconventional behavior of the time evolution of the systems, induced by multiple-spin interactions, reflects quantum information scrambling measured by the TMI. Furthermore, one may wonder how the magnitude of the hopping term,  $H_{\text{hop}}$ , changes the dynamics of the TMI for both 3-body and 4-range models. We shall address these problems by the numerical methods in the following sections.

#### IV. NUMERICAL INVESTIGATION OF DYNAMICS OF TMI

In this section, we shall show numerical results of the TMI for the models,  $H_{\text{XXZ}}$ ,  $H_{3\text{B}}$  and  $H_{4\text{R}}$ . In numerical calculation, we put  $\hbar = 1$ , set the parameters as  $v = 0.2$  and for  $H_{\text{XXZ}}$  and  $H_{3\text{B}}$ ,  $J_1 = 0.3$ , and for  $H_{3\text{B}}$ ,  $J_2 = J_3 \equiv J_0$  with a varying parameter  $J_0$ . We also employ Quspin package [44] in generating the time evolution operator of the target Hamiltonians. We focus on two observing time intervals: (I) early-time evolu-

tion where the time interval is set  $t_I \leq 10$ , which is less than the time  $(\hbar L)/2(\max(v/2, J_1, J_0))$  at which an excitation from the center of the system almost reaches the edges. (II) late-time evolution where the time interval is set  $t_{II} \leq 200$ , much larger than the time  $(\hbar L)/2(\max(v/2, J_1, J_0))$ . During that time interval, the TMI almost saturates as shown later. In our numerical resource, the accessible system size of the calculation of the TMI is up to  $L = 14$  and both open and periodic boundary conditions (OBC and PBC) are employed. We think that the early-time evolution is not affected substantially by the finite-size and boundary effects. On the other hand, the long-time evolution is affected by both of them, but we expect that the data give useful insight into the spread of information in a finite-size system since some experimental systems to be prepared to simulate our target spin models is obviously a finite-size system.

### A. Early-time evolution of TMI in XXZ and 3-body models

Let us move on numerical calculation of the TMI in early-time evolution for the XXZ and 3-body models. For the 3-body model of  $H_{3B}$ , we set  $J_0 = 2$ , where the level-spacing analysis (LSA) of the 3-body model indicates that the model is in the nearly-integrable regime (See Appendix B). It is interesting how such near-integrability reflects the early-time evolution of the TMI. As a reference value of the time evolution of the TMI, we use values of the Haar random unitary numerically obtained as,  $I_3^H/L = -8.559, -10.5576$  and  $-12.5566$  for  $L = 10, 12$  and  $14$ , respectively.

Figure 2 shows the early-time evolution of  $\tilde{I}_3$  in the 3-body model. For both PBC and OBC, [Figs. 2 (a) and 2 (b)],  $\tilde{I}_3$  starts to decrease with oscillation [45], and it stays negative indicating the spread of information over the entire system. We find the increase of  $-\tilde{I}_3$  is logarithmic-like. On the other hand, figure 3 shows the early-time evolution of  $\tilde{I}_3$  in the XXZ model. For both PBC and OBC [Figs. 3 (a) and 3 (b)],  $\tilde{I}_3$  starts to decrease linearly with time. This linear light-cone decrease of the TMI is similar to the linear light-cone increase in BEE [46] and also the operator entanglement entropy shown in Ref.[23].

Our numerical results indicate the time-evolution behavior of the TMI is changed by the presence of the interactions described by  $J_2$  and  $J_3$  terms, i.e., from linear to logarithmic-like decrease. This change has also been observed in the time evolution of the BEE for many-body wave functions with a fixed product initial state. In this sense, the TMI of the time-evolution operator exhibits similar behavior to the BEE at least in early-time dynamics.

We also numerically investigated the mutual information  $I(A : C)$ , and the results are shown in Appendix C. Similar behavior to the above TMI is observed by measuring entanglement velocity (Tsunami velocity). But,

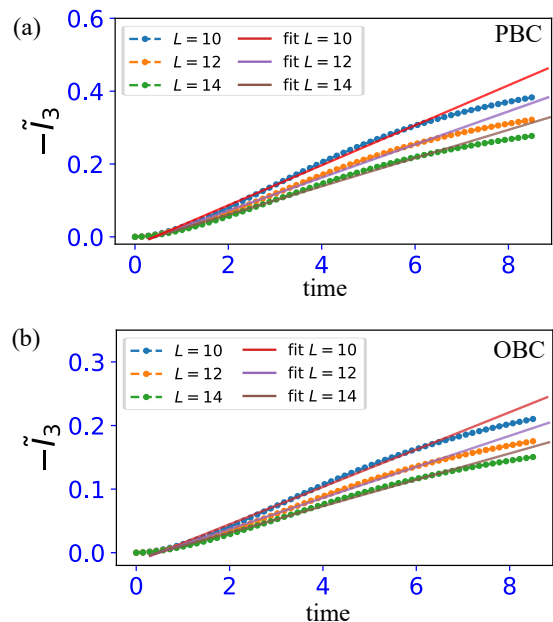


FIG. 3. Early-time evolution of XXZ model. (a) The result of PBC case. The linear fitting lines are  $(-\tilde{I}_3) = 0.0549t - 0.0231$ ,  $(-\tilde{I}_3) = 0.0459t - 0.0199$  and  $(-\tilde{I}_3) = 0.0395t - 0.0174$  for  $L = 10, 12$  and  $14$ , respectively. (b) The result of OBC case. The linear fitting lines are  $(-\tilde{I}_3) = 0.0295t - 0.0145$ ,  $(-\tilde{I}_3) = 0.0246t - 0.0121$  and  $(-\tilde{I}_3) = 0.0211t - 0.0105$  for  $L = 10, 12$  and  $14$ , respectively. We set  $v = 0.2$  and  $J_1 = 0.3$ . In the fitting, we used the data points within  $t \in [0.28 : 6.94]$ .

please note that this correspondence does not necessarily imply that slow-dynamics of the system emerges with suppression of the negativity in  $\tilde{I}_3$  for late-time evolution. This issue will be discussed after looking at the numerical results of the late-time evolution.

### B. Late-time evolution of TMI

Next, we show the numerical results of the late-time evolution of the TMI for the XXZ and 3-body models. Contrary to the study on large-size systems, our calculation includes finite-size and boundary effects, and consequently, a saturation of the TMI takes place to a certain finite value. Nonetheless, the detailed study of late-time evolution even for finite-size systems may be useful for future experiments as the system size there is obviously finite, and it is important to numerically observe how the target models of finite-size systems behave specifically compared to general expectations for infinite systems (i.e., the thermodynamic limit).

Figure 4 shows the late-time evolution of  $\tilde{I}_3$  in the 3-body model. For both PBC and OBC cases [Figs. 4 (a) and 4 (b)] and for all system sizes, the saturation of  $\tilde{I}_3$  takes place with a negative value. We find that for long-time evolution the obtained results of  $-\tilde{I}_3$  can be fitted

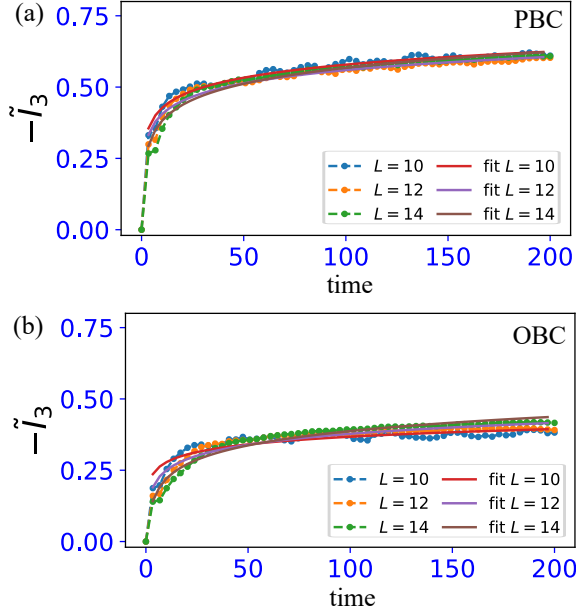


FIG. 4. Late-time evolution of the 3-body model. (a) The result of the PBC case. The fitting lines are  $(-\tilde{I}_3) = 0.0457 \log_2 t + 0.2748$ ,  $(-\tilde{I}_3) = 0.0465 \log_2 t + 0.2508$  and  $(-\tilde{I}_3) = 0.0560 \log_2 t + 0.1958$  for  $L = 10, 12$  and  $14$ , respectively. (b) The result of the OBC case. The fitting lines are  $(-\tilde{I}_3) = 0.0269 \log_2 t + 0.1889$ ,  $(-\tilde{I}_3) = 0.0384 \log_2 t + 0.1226$  and  $(-\tilde{I}_3) = 0.0504 \log_2 t + 0.0535$  for  $L = 10, 12$  and  $14$ , respectively. We set  $J_1 = 0.3$ ,  $J_0 = 2$  and  $v = 0.2$ . In the fitting, we used the data points within  $t \in [2.5 : 200]$ .

by a logarithmic-like function quite well. Also, for this parameter regime, the system-size dependence of saturation values is small. This implies that the saturation value of the TMI,  $I_3$ , in the late-time evolution scales with  $\mathcal{O}(L)$ , since the TMI of the Haar random unitary  $I_3^H$  almost scales with  $\mathcal{O}(L)$ . Thus,  $\tilde{I}_3$  has only negligibly small system-size dependence.

On the other hand, figure 5 shows the late-time evolution of  $\tilde{I}_3$  in the XXZ model. For both PBC and OBC [Figs. 5 (a) and 5 (b)],  $\tilde{I}_3$  starts to decrease linearly in early-time and it fairly slows down the negative growth until  $(\hbar L)/2(\max(v/2, J_1))$ . Finally, for both PBC and OBC cases,  $\tilde{I}_3$  almost saturates with a negative value within the time-interval. This break-down behavior is similar to the behavior of the OEE obtained in Ref.[23].

In addition, we note that for the OBC case, the system-size dependence of  $\tilde{I}_3$  is somewhat larger than that of the PBC case. We expect that this comes from finite-size and boundary effects.

### C. Observation of the TMI dynamics for 4-range model

Let us turn to the TMI in the 4-range model. An analytical perturbation theory in the previous work [24] indi-

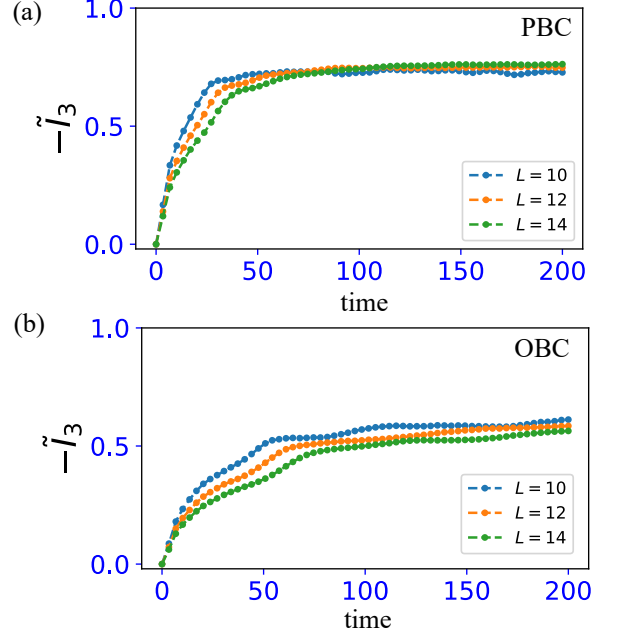


FIG. 5. Late-time evolution of the XXZ model for the PBC case [(a)] and OBC case [(b)]. We set  $v = 0.2$  and  $J_1 = 0.3$ .

cates that the 4-range model can exhibit a slower-increase of the BEE compared to that of the 3-body model. In what follows, we set all the couplings to the same value, such as  $t_2 = t_3 = t_4 \equiv t_0$ . We carried out the LSA with the result in Appendix B, which shows that for large  $t_0$ , the LSA deviates from the Wigner-Dyson distribution and it gets behavior close to that of integrable models for large  $L$ .

We observe early-time evolution as varying  $t_0$  with  $v = 0.2$ . The results for both PBC and OBC are shown in Fig. 6. We find that for both PBC and OBC cases, the negative growth of  $\tilde{I}_3$  changes from linear-like to logarithmic-like as increasing  $t_0$ . In addition, we observe that for sufficiently large  $t_0$  (i.e., see  $t_0 = 2$  case in Fig. 6 (a)), the negative growth tends to deviate from the logarithmic behavior. Anyway, the multiple-spin interactions clearly affect the time evolution of the TMI in the early-time period. For late-time evolution for a large  $t_0$ , the decrease of the TMI is the same as that in the 3-body case, that is, the growth can be fitted by a logarithmic-like function satisfactorily (not shown).

## V. SATURATION VALUE

The numerical results of the late-time evolution exhibit saturation of  $\tilde{I}_3$ . In the finite-size system, it is important to see how such a saturation value depends on the parameters, system size, and integrability. Here we focus on the PBC case and we plot the time-averaged value of  $\tilde{I}_3$  in  $100 \leq t \leq 200$  for various system sizes and parameters



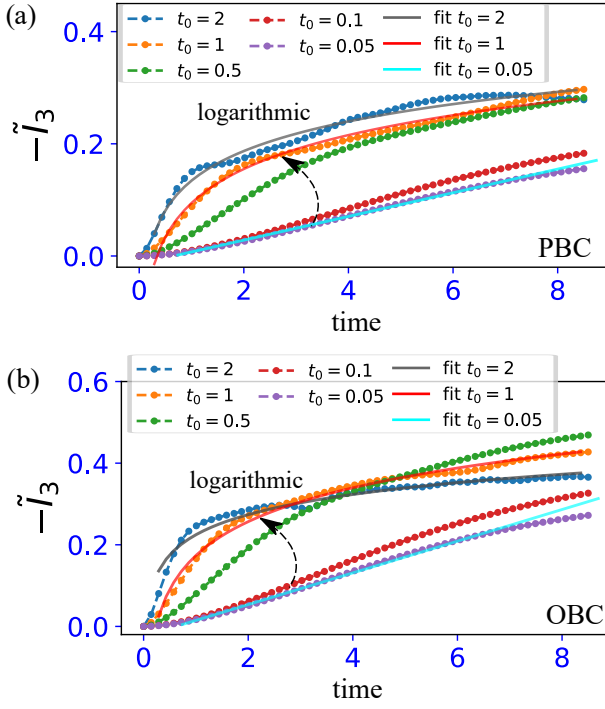


FIG. 6. Early-time evolution of the 4-range model. (a) PBC case. The fitting lines are  $(-\tilde{I}_3) = 0.0494 \log_2 t + 0.2246$ ,  $(-\tilde{I}_3) = 0.0829 \log_2 t + 0.1737$  and  $(-\tilde{I}_3) = 0.0402t - 0.0260$  for  $t_0 = 2$ ,  $t_0 = 1$  and  $t_0 = 0.05$ . (b) OBC case.  $(-\tilde{I}_3) = 0.0527 \log_2 t + 0.1344$ ,  $(-\tilde{I}_3) = 0.0606 \log_2 t + 0.0945$  and  $(-\tilde{I}_3) = 0.0217t - 0.0158$  for  $t_0 = 2$ ,  $t_0 = 1$  and  $t_0 = 0.05$ . We used the data points within  $t \in [0.25 : 8.5]$  and  $t \in [0.7 : 5.7]$  for the logarithmic fitting and linear fitting, respectively. For the data  $t_0 = 2$ , at the time scale  $t \sim 1/t_0 = 0.5$ , the curvature of the behavior of the TMI takes a peak.  $L = 12$ .

in the 3-body and 4-range models, as in all values of the parameters,  $\tilde{I}_3$  is almost saturated after  $t = 100$ . We denote the averaged value  $\langle \tilde{I}_3 \rangle$ . In calculations, we broadly vary the parameters  $J_0$  and  $t_0$ , and the integrability of the 3-body and 4-range models is examined by using the LSA [see Appendix B]. We also take three system sizes,  $L = 10, 12$ , and  $14$  for the observation.

We summarize the absolute values  $|\langle \tilde{I}_3 \rangle|$  for the 3-body model shown in Figs. 7 (a) and 7 (b) and for the 4-range models in Figs. 7 (c) and 7 (d), respectively. For  $L = 10$  ( $1/L = 0.10$  line in Fig. 7 (a)), there is a clear relationship between the saturation values and the integrability estimated by the LSA: In Figs. 7 (a) and 7 (b) for larger  $J_0$ , where the model tends to be integrable,  $|\langle \tilde{I}_3 \rangle|$  is suppressed. Also compared to that of the XXZ model (nonlocalized integrable model)  $|\langle \tilde{I}_3 \rangle|$  at small  $J_0 \leq 0.5$  is larger than that of the XXZ model, indicating the weak multiple-spin interactions enhance the negativity of the TMI. This behavior of the TMI follows the results of the LSA as shown in Appendix B and it implies that for weak multiple-spin interactions, the 3-body model exhibits non-integrable and the ETH

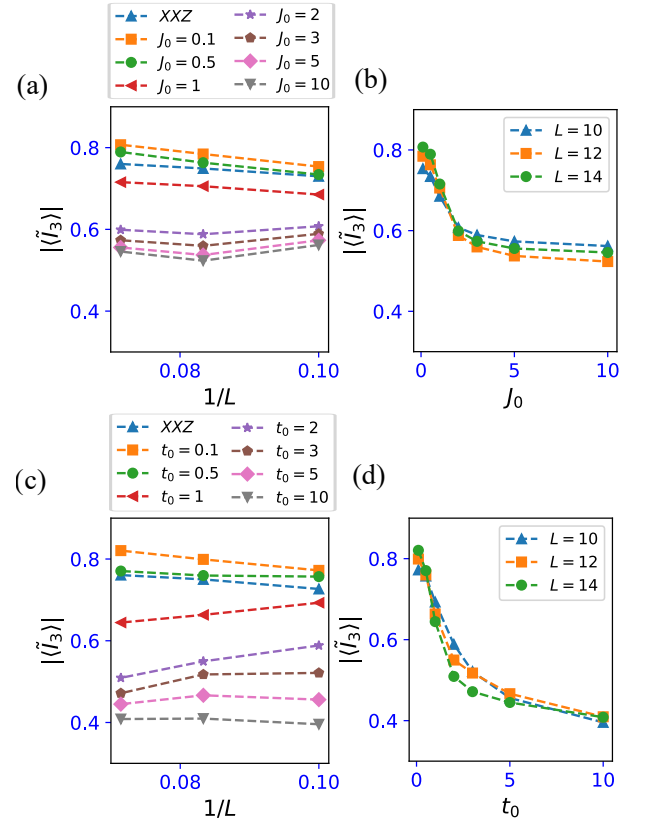


FIG. 7. Time average of the TMI for late-time evolution. (a) and (b): the data of the TMI vs system size  $L$  and the data of the TMI vs  $J_0$  for the 3-body case. In data (b), the data lines of three different system sizes cross at  $\sim 1.5$ . This is a qualitative signature of a phase transition. (c) and (d): the data of the TMI vs system size  $L$  and the data of the TMI vs  $J_0$  for the 4-range case. We plot the averaged value of the TMI for  $100 \leq t \leq 200$ . We used the data of the PBC case. We set  $v = 0.2$ ,  $J_1 = 0.3$ .

tendency. Similar phenomenon was observed in Ref. [33], which shows the XXZ model tends to get the ETH behavior by a local integrability-breaking perturbation, where Wigner-Dyson distribution of energy levels was also observed there [47, 48]. The above trends of the TMI also appear in the case  $L = 12$  and  $14$  cases as shown in Fig. 7 (a). We note that even for large  $J_0$ , the value of  $|\langle \tilde{I}_3 \rangle|$  is not strongly suppressed (fairly deviates from zero). This result indicates the limits on determining how strongly the TMI is suppressed by the interactions.

We also find that the gap of  $|\langle \tilde{I}_3 \rangle|$ 's between  $J_0 = 1$  and  $J_0 = 2$  data is large, in accordance with the behavior of the LSA, which indicates that the system changes its character from non-integrable to integrable with the increase in the strength of the multiple-spin interactions. Hence, there may exist something like a phase transition or crossover between  $J_0 = 1$  and  $2$ , which reflects the TMI. We plot the  $|\langle \tilde{I}_3 \rangle|$  vs  $J_0$  for three different system sizes in Fig. 7 (b). The three data curves seem to cross

with each other at  $J_0 \sim 1.5$ . This can be a sign of a critical phase transition point in this model. In this sense, the estimation of the saturation value of the TMI may be useful for detecting a phase transition from the viewpoint of the information spread and scrambling, which has been already suggested in the measurement induced phase transition context [49].

The above properties of the 3-body model also exist in the 4-range model as shown in Fig. 7 (c). This behavior of the TMI follows the results of the LSA as shown in Appendix B. For large  $t_0 (\gtrsim 1)$ , the values of  $|\langle \tilde{I}_3 \rangle|$  are smaller than those of the 3-body case ( $J_0 (\gtrsim 1)$ ). This indicates the 4-range terms induce stronger suppression than the 3-body terms. We also observe that the difference of  $|\langle \tilde{I}_3 \rangle|$  between  $t_0 = 0.5$  and  $t_0 = 2$  is rather large with fixed  $L$ . This again indicates the presence of a phase transition. However, as long as we plot the  $|\langle \tilde{I}_3 \rangle|$  vs  $t_0$  for the three different system sizes in Fig. 7 (d), the result is different from the 3-body case in Fig. 7 (b). The three curves with different  $L$ 's do not seem to cross with each other at single point  $t_0$ . In this sense, we cannot say that there is a distinct phase transition through this finite system-size investigation accessible in our numerical resource. However, we shall briefly comment on this point later on.

Summarizing the above observations, we conclude that the degree of integrability, measured by the LSA, is related to the degree of the scrambling observed by the TMI for the present disorder-free 3-body and 4-range models. The results obtained in this paper do not agree with the observation in [26], where the non-existence of relationship between integrability and the degree of the scrambling, but agree with the observation in the study in the MBL system [29, 30], where the relationship between integrability and the degree of the scrambling exists. Therefore, more detailed investigation is needed to obtain universal understanding of the relationship between the integrability and information scrambling for both the MBL and ETH systems.

Here, we comment that the multiple-spin operators in the 3-body and 4-range models are also conserved quantities for  $v = 0$ . The system with a finite  $v$  approaches a nearly integrable system as these interactions are getting strong. However, these interactions are not single-site operators but non-local ones. Such a non-local conserved quantity can enhance the spread of information. We speculate that the combination of non-locality of these non-local multiple-spin interactions and the small hopping  $H_{\text{hop}}$  may inhibit strong suppression ( $|\langle \tilde{I}_3 \rangle| \ll 1$ ). For this point, the previous study [24] gave a similar expectation: The 3-body model indeed exhibits quasi-localization, even for large multiple-spin interactions, and the final value of the BEE exhibits thermal value in the thermodynamic limit.

Another comment concerns the finite system size. One may wonder that the above observation for the existence of the crossover/ phase transition between the ETH and nearly-integrable regimes is simply a finite-size effect

and it disappears in the thermodynamic limit. Very recently, however, an interesting observation was proposed in which such a kind of crossovers survive in a *dynamic limit* [32]. To approach the dynamic limit, the parameters of the Hamiltonian must be scaled with the system size. By doing an appropriate scaling, chaos (ETH)-localization transition is to be observed. For the present models, the scaling law of the parameters is a future problem, although similar quantum spin models are studied in Ref. [32]. However, the data of the 4-body model shown in Fig. 7 (d),  $|\langle \tilde{I}_3 \rangle|$  vs  $t_0$ , seem to indicate a phase transition or crossover in a dynamic limit. That is, by suitable scaling of  $t_0$  with system size  $L$ , the three curves may collapse to a single curve [32], although investigation for various system sizes is needed to verify that.

## VI. DISCUSSION AND CONCLUSION

We numerically investigated the spread of information and scrambling by the unitary time evolution operator of some disorder-free spin models with multiple-spin interactions. The TMI is a suitable quantitative observable to quantify the spread of information and scrambling. Even in a finite-size system, the TMI exhibits non-trivial growth in early-time. For weak hopping, we found the negative increase of the TMI is logarithmic-like in contrast to the linear light-cone growth in the integrable XXZ model. The multiple-spin interactions induce logarithmic-like modification for the spread of information.

We also numerically investigated the late-time evolution of the TMI in the finite-size systems, where our accessible system size is up to  $L = 14$ . We observed that the saturation values of the TMI for various parameters in the present disorder-free spin models clearly depend on integrability estimated by the LSA. This implies that integrability nature of the system exhibits a strong correlation with the degree of the scrambling measured by the TMI. In addition, the non-local quasi-conserved quantity corresponding to the multiple-spin operators in the multiple-spin interactions may inhibit strong suppression of the TMI ( $|\langle \tilde{I}_3 \rangle| \ll 1$ ). The effect of the magnitude of “ $\ell$ -bit” on the TMI is under study by using other models, and results are to be reported in a near-future [50]. Compared to the MBL case [29, 30], our numerical results indicated that the strong suppression of the TMI does not occur in our models.

Nevertheless, we must be careful to take our conclusions obtained from numerical observations to be very general and definitive, because our numerical results are far from the thermodynamic limit. The study of the TMI for larger system sizes by alternative numerical schemes will be future work, in particular, to verify our findings in the study of late-time dynamics. An MPO approach [15] may be efficient for this end.

*Acknowledgements.*— This work is supported by JSPS



KAKEN-HI Grant Number JP21K13849 (Y.K.) and T.O. has been supported by the Program for Developing and Supporting the Next-Generation of Innovative Researchers at Hiroshima University.

## APPENDIX A: TIME INDEPENDENT PART OF ENTROPY IN CALCULATION OF THE TMI

In this work, we focus on zero-magnetization sector of the spin Hilbert space, with not  $2^L$  dimension but  $\binom{L}{L/2}$ -dimension and consider that all subsystems A, B, C, and D are equal, that is, including  $L/2$ -lattice sites. Then, the OEE  $S_{X_1}$  ( $X_1 = A, B, C, D$ ) is given by

$$S_{X_1} = - \sum_{n_D=0}^{L/2} \binom{L/2}{n_D} g(n_D) \log_2 g(n_D), \quad (9)$$

where  $g(n_D) = \binom{L/2}{n_D} / N_D$  ( $N_D$  is total Hilbert space dimension,  $\binom{L}{L/2}$ ).

As far as all subsystems A, B, C and D are equal, the  $S_X$  is time-independent [22, 29], hence, we only need to calculate  $S_{AC}$  and  $S_{AD}$ , which are time-dependent in the calculation of the TMI.

## APPENDIX B: LEVEL SPACING ANALYSIS

In this appendix, we investigate the integrability of both 3-body and 4-range models by applying level spacing analysis (LSA) [51, 52]. Being integrable or not is determined by the values of  $J_2$ , and  $J_3$  in the 3-body model and the values of  $t_\alpha$  in the 4-range model. Since we expect that the integrability property does not depend on the boundary condition, we here employ the periodic boundary condition (PBC).

To extract the integrable properties of the model straightforwardly, we diagonalize the Hamiltonian of the models in a sector with a fixed momentum and the parity,  $+1$ , since the models are translational invariant and

invariant to the parity operation. Here we employ QuSpin solver [44] to diagonalize the Hamiltonian. Then we take all eigenvalues of Hamiltonian in each momentum sector and calculate the level spacing  $r_s^k$  defined by  $r_s^k = [\min(\delta_k^{(s)}, \delta_k^{(s+1)})] / [\max(\delta_k^{(s)}, \delta_k^{(s+1)})]$  for  $s$ , where  $\delta_k^{(s)} = E_{s+1}^k - E_s^k$  and  $\{E_s^k\}$  is the set of energy eigenvalues in ascending order in momentum sector  $k$  and  $s$  labels the elements of eigenvalues of the Hamiltonian in momentum sector  $k$ . We average over the suffix  $s$  and obtain each mean-level spacing  $\langle r \rangle_k$  in each momentum sector.

In general, if the system is integrable, the average level spacing takes  $\langle r \rangle \simeq 0.39$ , corresponding to the Poisson distribution. On the other hand, if the system is non-integrable (chaotic), the average level spacing takes  $\langle r \rangle \simeq 0.53$ , corresponding to the Wigner-Dyson (WD) distribution [51, 52].

By varying  $J_0 (= J_2 = J_3)$  for the 3-body model and  $t_0 (= t_\alpha)$  for 4-range model, we observed how  $\langle r \rangle$  behaves. Figure 8 (a) shows the result of the 3-body case. Here, we average over the suffix  $k$  and obtain the total averaged value over  $k$ ,  $\langle r \rangle$ . For small  $J_0$ , where the hopping term is dominant,  $\langle r \rangle$  is close to the value of the WD distribution. Thus, the system is non-integrable. As increasing  $J_0$ , we observe that  $\langle r \rangle$  approaches the value of the Poisson distribution. This indicates that the 3-body model approaches being integrable.

Next, we turn to the results of the 4-range model in Fig. 8 (b). Here, we show the result of zero momentum sector  $k = 0$ . For small  $t_0$ ,  $\langle r \rangle$  is close to the value of the WD distribution. But the deviation is large for small  $L$ . Entirely, the system tends to be non-integrable. As increasing  $t_0$ , we observe that  $\langle r \rangle$  deviates from the value of the WD distribution. For large  $L$  the value well approaches the value of the Poisson distribution. For small  $L$ , the value decreases up to a value less than that of the Poisson distribution. Hence, the thermodynamic limit, the system is integrable for large  $t_0$ . Even for small  $L$  and large  $t_0$ , the system is not non-integrable at least.

These LSA results are almost consistent with the expectation in the previous work [24].

## APPENDIX C: ENTANGLEMENT VELOCITY IN 3-BODY AND 4-RANGE MODELS

In this appendix, we numerically observe the time evolution of the mutual information  $I(A : C)$  defined by Eq.(2) in Sec. II. In dynamics in general chaotic system,  $I(A : C)$  starts from a certain finite value [22] and then linearly decreases. Therefore,  $I(A : C)$  behaves as  $I(A : C)(t) = I(A : C)(t = 0) - v_E t$ , where  $s = 2$  in spin  $1/2$  bases and  $v_E$  is entanglement velocity (sometimes called Tsunami velocity).

We investigate whether or not such a linear decrease appears in our model or how such a linear decrease changes by varying the parameters  $J_0$  and  $t_0$  in the 3-body or 4-range models. We here focus on early-time

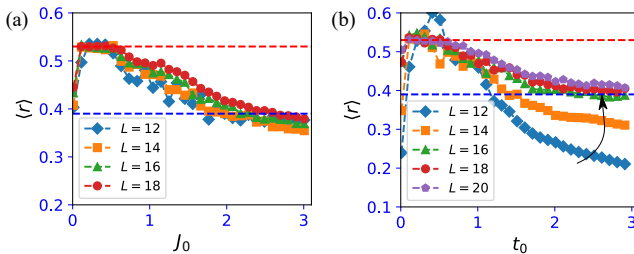


FIG. 8. Level spacing ratio for 3-body model [(a)] and 4-range model [(b)].  $t_2 = t_3 = t_4 = t_0$ . We set  $L = 12-18$  [(a)] and  $L = 12-20$  [(b)],  $J_1 = 0.3$  and  $v = 0.2$ . The red and blue dashed lines represent the WD value 0.53 and the Poisson value 0.39.

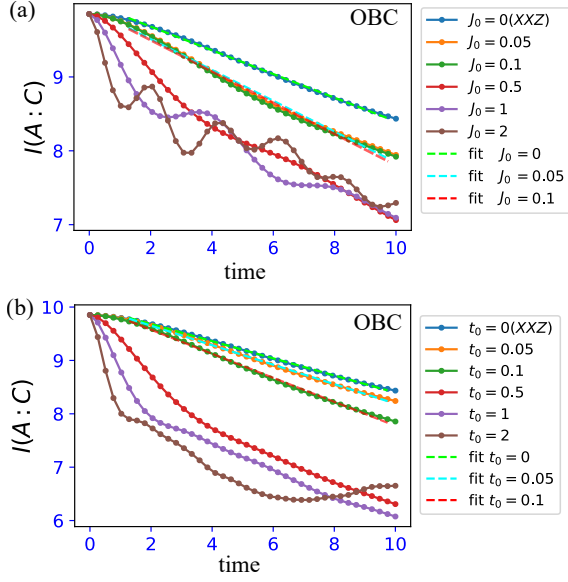


FIG. 9. (a) Early-time evolution of mutual information  $I(A : C)$  of 3-body [(a)] and 4-range models [(b)]. We used OBC. In the result (a), the linear fitting lines are  $I(A : C) = -0.1606t + 10.0032$ ,  $I(A : C) = -0.2090t + 9.9318$  and  $I(A : C) = -0.2118t + 9.9214$  for  $J_0 = 0(XXZ)$ ,  $J_0 = 0.05$  and  $J_0 = 0.1$ , respectively. In the result (b), the linear fitting lines are  $I(A : C) = -0.1825t + 10.0157$  and  $I(A : C) = -0.2250t + 10.0247$  for  $t_0 = 0.05$  and  $t_0 = 0.1$ .

evolution under OBC, and focus on  $L = 12$  system size.

Figure 9 is the time evolution of  $I(A : C)$  for various parameters. For all data in both Fig. 9 (a) and Fig. 9 (b),  $I(A : C)$  starts from a constant value obtained by Eq. (9) and  $S_{AC} = 0$  at  $t = 0$ . See the 3-body case in Fig. 9 (a), for small  $J_0$ ,  $I(A : C)$  almost linearly decreases and a linear fitting can be applied and the entanglement velocity can be extracted. The value  $v_E$  obtained by the data is close to the hopping value  $v/2$ . But for large  $J_0$ , the linear decrease breaks down and the linear fitting is of course no longer applied or we cannot extract  $v_E$ , non-trivial decrease with oscillation appears. We expect that this behavior comes from the non-locality of the multiple-spin interactions, i.e., not only NN ‘hopping of domain walls’ but also multi-distance terms give non-trivial effects on the short-range scrambling of the information.

The same behavior is observed in the 4-range model as shown in Fig. 9 (b). For small  $t_0$ , the linear fitting of  $I(A : C)$  can be applied and the entanglement velocity can be extracted. The value  $v_E$  obtained by the data is close to the hopping value  $v/2$ . But for large  $t_0$ , such a linear decrease breaks down.

- 
- [1] P. Hayden and J. Preskill, J. High Energy Phys. 09 (2007) 120.
  - [2] Y. Sekino and L. Susskind, J. High Energy Phys. 10 (2008) 065.
  - [3] S. H. Shenker and D. Stanford, J. High Energy Phys. **2014**, 1 (2014).
  - [4] J. Maldacena, S. H. Shenker, and D. Stanford, J. High Energy Phys. **2016**, 1 (2016).
  - [5] R. Nandkishore, and D. A. Huse, Annual Review of Condensed Matter Physics **6**, 15 (2015).
  - [6] D. A. Abanin, E. Altman, I. Bloch, and M. Serbyn, Rev. Mod. Phys. **91**, 021001 (2019).
  - [7] D. M. Basko, I. L. Aleiner, and B. L. Altshuler, Ann. Phys. **321**, 1126 (2006).
  - [8] J. H. Bardarson, F. Pollmann, and J. E. Moore, Phys. Rev. Lett. **109**, 017202 (2012).
  - [9] M. Rigol, V. Dunjko, V. Yurovsky, and M. Olshanii, Phys. Rev. Lett. **98**, 050405 (2007).
  - [10] C. Gogolin and J. Eisert, Reports Prog. Phys. **79**, 056001 (2016).
  - [11] B. Swingle and D. Chowdhury, Phys. Rev. B **95** 060201 (2017).
  - [12] R. Fan, P. Zhang, H. Shen, and H. Zhai, Sci. Bull. **62**, 707 (2017).
  - [13] Y. Huang, Y.-L. Zhang, and X. Chen, Annalen der Physik **529**, 1600318 (2017).
  - [14] S. Sahu, S. Xu, and B. Swingle, Phys. Rev. Lett. **123**, 165902 (2019)
  - [15] D. J. Luitz and Y. Bar Lev, Phys. Rev. B **96**, 020406 (2017).
  - [16] C. -J. Lin and O. I. Motrunich, Phys. Rev. B **97**, 144304 (2018).
  - [17] M. Knap, Phys. Rev. B **98**, 184416 (2018).
  - [18] D. Hahn, P. A. McClarty, and D. J. Luitz, SciPost Phys. **11**, 074 (2021).
  - [19] A. Bohrdt, C. B. Mendl, M. Endres, and M. Knap, New J. Phys. **19**, 063001 (2017).
  - [20] S. -S. Li, R. -Z. Huang, and H. Fan, arXiv: 2109.05537 (2021).
  - [21] L. Colmenarez and D. J. Luitz, Phys. Rev. Res. **2**, 043047 (2020).
  - [22] P. Hosur, X.-L. Qi, D. A. Roberts, and B. Yoshida, Journal of High Energy Physics 004 (2016).
  - [23] T. Zhou and D. J. Luitz, Phys. Rev. B **95**, 094206 (2017).
  - [24] A. A. Michailidis, M. Žnidarič, M. Medvedyeva, D.A. Abanin, T. Prosen, and Z. Papić, Phys. Rev. B **97**, 104307 (2018).
  - [25] I. MacCormack, M.T. Tan, J. Kudler-Flam, and S. Ryu, Phys. Rev. B **104**, 214202 (2021).
  - [26] E. Iyoda and T. Sagawa, Phys. Rev. A **97**, 042330 (2018).
  - [27] O. Schnaack, N. Bolter, S. Paeckel, S. R. Manmana, S. Kehrein, and M. Schmitt, Phys. Rev. B **100**, 224302 (2019).
  - [28] D. Wanisch and S. Fritzsche, Phys. Rev. A **104**, 042409 (2021).
  - [29] N. Bölter and S. Kehrein, Phys. Rev. B **105**, 104202

- (2022).
- [30] E. Mascot, M. Nozaki, and M. Tezuka, arXiv:2012.14609 (2020).
  - [31] A. Morningstar, L. Colmenarez, V. Khemani, D. J. Liutz, and D. A. Huse, arXiv:2107.05642.
  - [32] V. B. Bulchandani, D. Huse, and S. Gopalakrishnan, arXiv:2112.14762.
  - [33] M. Brenes, T. LeBlond, J. Goold, and M. Rigol, Phys. Rev. Lett. **125**, 070605 (2020).
  - [34] M. Žnidarč, Phys. Rev. Lett. **125**, 180605 (2020).
  - [35] A. J. Friedman, S. Gopalakrishnan, and R. Vasseur, Phys. Rev. B **101**, 180302 (2020).
  - [36] J. Durnin, M. J. Bhaseen, and B. Doyon, Phys. Rev. Lett. **127**, 130601 (2021).
  - [37] A. Hutsalyuk and B. Pozsgay, Phys. Rev. E **103**, 042121 (2021).
  - [38]  $I_3^H$  is calculated under the dimension  $2^L$  including full-sectors of total magnetization.
  - [39] J. K. Pachos and M. B. Plenio, Phys. Rev. Lett. **93**, 056402 (2004).
  - [40] H. P. Buchler, A. Micheli, and P. Zoller, Nat. Phys. **3**, 726 (2007).
  - [41] G. De Tomasi, D. Hetterich, P. Sala, and F. Pollmann, Phys. Rev. B **100**, **214313** (2019).
  - [42] W. -H. Li, X. Deng, and L. Santos, Phys. Rev. Lett. **127**, 260601 (2021).
  - [43] P. Sala, T. Rakovszky, R. Verresen, M. Knap, and F. Pollmann, Phys. Rev. X **10**, 011047 (2020).
  - [44] P. Weinberg and M. Bukov, SciPost Phys. **7**, 20 (2019); **2**, 003 (2017).
  - [45] This oscillation comes from the multiple-spin interaction terms. If we set  $v = 0$ , the TMI in the 3-body and 4-range models exhibits oscillating behavior.
  - [46] H. Kim and D.A. Huse, Phys. Rev. Lett. **111**, 127205 (2013).
  - [47] L. Santos, J. Phys. A **37**, 4723 (2004).
  - [48] L. F. Santos and A. Mitra, Phys. Rev. E **84**, 016206 (2011).
  - [49] A. Zabalo, M. J. Gullans, J. H. Wilson, S. Gopalakrishnan, D. A. Huse, and J. H. Pixley, Phys. Rev. B **101**, 060301 (2020).
  - [50] T. Orito, Y. Kuno, and I. Ichinose, in preparation.
  - [51] V. Oganesyan and D.A. Huse, Rev. B **75**, 155111 (2007).
  - [52] A. Pal and D. A. Huse, Phys. Rev. B **82**, 174411 (2010).